Long-term Characterization of Retinal Degeneration in Royal College of Surgeons Rats Using Spectral-Domain Optical Coherence Tomography

Renee C. Ryals,[1] Michael D. Andrews,[1] Shreya Datta,[1] Aaron S. Coyner,[1] Cody M. Fischer,[1] Yuquan Wen,[2] Mark E. Pennesi,[1] and Trevor J. McGill[1,3]

[1]Casey Eye Institute, Oregon Health & Science University, Portland, Oregon, United States
[2]Baylor University Medical Center, Dallas, Texas, United States
[3]Department of Neuroscience, Oregon National Primate Research Center, Oregon Health & Science University, Beaverton, Oregon, United States

Correspondence: Renee C. Ryals, Casey Eye Institute, 3375 SW Terwilliger Boulevard, Portland, OR 97239, USA; ryals@ohsu.edu.

Submitted: July 20, 2016
Accepted: January 24, 2017

Citation: Ryals RC, Andrews MD, Datta S, et al. Long-term characterization of retinal degeneration in Royal College of Surgeons rats using spectral-domain optical coherence tomography. *Invest Ophthalmol Vis Sci*. 2017;58:1378–1386. DOI:10.1167/iovs.16-20363

Purpose. Prospective treatments for age-related macular degeneration and inherited retinal degenerations are commonly evaluated in the Royal College of Surgeons (RCS) rat before translation into clinical application. Historically, retinal thickness obtained through postmortem anatomic assessments has been a key outcome measure; however, utility of this measurement is limited because it precludes the ability to perform longitudinal studies. To overcome this limitation, the present study was designed to provide a baseline longitudinal quantification of retinal thickness in the RCS rat by using spectral-domain optical coherence tomography (SD-OCT).

Methods. Horizontal and vertical linear SD-OCT scans centered on the optic nerve were captured from Long-Evans control rats at P30, P60, P90 and from RCS rats between P17 and P90. Total retina (TR), outer nuclear layer+ (ONL+), inner nuclear layer (INL), and retinal pigment epithelium (RPE) thicknesses were quantified. Histologic sections of RCS retina obtained from P21 to P60 were compared to SD-OCT images.

Results. In RCS rats, TR and ONL+ thickness decreased significantly as compared to Long-Evans controls. Changes in INL and RPE thickness were not significantly different between control and RCS retinas. From P30 to P90 a subretinal hyperreflective layer (HRL) was observed and quantified in RCS rats. After correlation with histology, the HRL was identified as disorganized outer segments and the location of accumulated debris.

Conclusions. Retinal layer thickness can be quantified longitudinally throughout the course of retinal degeneration in the RCS rat by using SD-OCT. Thickness measurements obtained with SD-OCT were consistent with previous anatomic thickness assessments. This study provides baseline data for future longitudinal assessment of therapeutic agents in the RCS rat.

Keywords: spectral-domain optical coherence tomography, Royal College of Surgeons Rat, animal models, inherited retinal degeneration, MERTK

Retinal degenerative diseases such as age-related macular degeneration (AMD) and retinitis pigmentosa (RP) are defined by the progressive degeneration of the neural retina, resulting in severe visual loss and often legal blindness.[1–3] Pathology in AMD and some forms of RP can involve dysfunction of the retinal pigment epithelium (RPE).[1–3] Multiple animal models have been used to investigate such RPE dysfunction and test potential therapies.[4–7] One prominent photoreceptor degeneration model that is often used to determine the safety and efficacy of prospective AMD and RP therapies is the Royal College of Surgeons (RCS) rat.[8] The RCS rat has a mutation in the *merTK* gene that renders RPE cells unable to phagocytose shed photoreceptor outer segments at a normal rate,[6–9] ultimately leading to photoreceptor cell death and progressive vision loss.[10,11]

Previous reports[8,12–15] have thoroughly documented the progressive photoreceptor degeneration in RCS rats by using anatomic methods. By 3 weeks of age, photoreceptor outer segments show evidence of disruption with the development of an apical debris zone. By 4 weeks, an increased number of pyknotic cells are observed as the outer nuclear layer begins to degenerate.[8,9] At 7 weeks, approximately 50% of the photoreceptor nuclei have degenerated. By 12 weeks, the outer nuclear layer has been reduced to a single layer of photoreceptor cell bodies and the debris zone occupies the former outer segment area.[8,9] This debris zone eventually deteriorates, allowing the inner nuclear layer (INL) to come in close contact with the RPE by 24 weeks of age.[8,9] Subsequent secondary neurodegenerative changes occur in the inner retina at late stages, including the loss of retinal ganglion cells, withdrawal of bipolar cell axons, Müller cell gliosis, and neuronal sprouting of horizontal cells.[16–18]

In addition to documenting RCS retinal degeneration, many postmortem anatomic assessments have provided the foundation for determining the efficacy of cell, gene, and pharmacologic therapies.[11,19–27] More recently, anatomic assessments have been combined with quantitative measurements of visual

function.[10,28] However, while visual thresholds could be measured longitudinally, only a single anatomic data point for each animal is possible, which precludes the ability to perform longitudinal studies in all subjects. The advent of spectral-domain optical coherence tomography (SD-OCT) has enabled the detailed analysis of retinal structure in vivo.[29–31] Spectral-domain OCT has been used successfully to characterize the long-term retinal degeneration in mouse (*rd1*, *rd10*, *Rho*$^{-/-}$, *Rpe65*$^{-/-}$) and rat (Rho P23H) models of inherited retinal degeneration.[32–34] Furthermore, multiple studies[35–38] have used retinal thickness measurements obtained from SD-OCT images as quantifiable therapeutic outcome measurements. Even though the RCS rat is widely used for retinal degeneration therapy development, an SD-OCT natural history study has not been performed and studies continue to use postmortem anatomic assessments to assess therapeutic outcomes.[19,20,22] Therefore, we characterized the progressive photoreceptor degeneration in the RCS rat by using SD-OCT over the first 3 months of life, during which time the outer nuclear layer degenerates. This longitudinal in vivo quantification of retinal degeneration in the RCS rat, using SD-OCT, will provide a baseline for future evaluations of prospective cell, gene, or pharmacologic therapies.

Methods

Animals

Pigmented RCS rats (RCS-p+/Lav) were used for this study. Wild-type, pigmented Long-Evans (LE) rats, obtained from Charles River (Seattle, WA, USA), were used as controls because although the retina layers thin with age, there is no appreciable cell loss or change in total retinal volume.[39] In addition, LE rats have previously been used to back breed pigment in the RCS line and to generate the nondystrophic RCS line.[40] Rats were housed in standard conditions under a 12/12-hour light–dark cycle (light cycle: ~200 lux). All experiments were approved by the Institutional Animal Care and Use Committee at OHSU and adhered to the ARVO Statement for the Use of Animals in Ophthalmic and Vision Research.

Imaging

RCS rats were imaged weekly from P17 to P60 and final images were obtained at P90. Both right (OD) and left (OS) eyes were imaged from 7 to 10 different RCS rats at each time point. Long-Evans control rats were imaged at P30, P60, and P90. Both OD and OS were imaged from four different LE rats at each time point. Before imaging, pupils were dilated with 1% tropicamide and 2.5% phenylephrine. Artificial tears were used throughout the procedure to maintain corneal clarity. Sedation was induced by ketamine (80 mg/kg)/xylazine (5 mg/kg). Spectral-domain OCT images were obtained by using the Envisu R2200-HR SD-OCT device (Bioptigen, Durham, NC, USA) with the reference arm placed at approximately 1187 mm. Single horizontal and vertical linear scans (2-mm preset scan width, 1500 a-scans/b-scan · 20 frames/b-scan) were obtained first while centered on the optic nerve, then with the nerve displaced either temporally/nasally or superiorly/inferiorly. To analyze interscan variability, three consecutive OD and OS temporal, nasal, superior, and inferior scans were obtained in three additional RCS rats at P30. Axial and transverse export resolution was 1.175 μm/pixel and 3.175 μm/pixel, respectively.

Image Processing and Segmentation

Spectra-domain OCT scans were exported from InVivoVue (Bioptigen, Inc., Morrisville, NC, USA) as AVI files. These files were loaded into ImageJ (version 1.45; provided in the public domain by the National Institutes of Health, Bethesda, MD, USA) where they then were registered by using the Stackreg plug-in and averaged as a z-stack. Manual segmentation and quantification of retinal layer thickness was performed with a custom-designed SD-OCT segmentation program built in IGOR Pro (IGOR Pro 6.12; WaveMetrics, Inc., Lake Oswego, OR, USA). Segmentation software is sharable with permission of the author (Yuquan Wen). For segmentation analysis, total retina (TR), INL, outer nuclear layer+ (ONL+), and RPE thicknesses were measured. The ONL+, the photoreceptor layer from the outer limiting membrane (OLM) to the INL/outer plexiform layer (OPL) interface, was used to enable consistent measurements across ages as hyperreflectivity in the photoreceptors increased. From P30 to P90, a hyperreflective layer (HRL) was observed and measured in RCS rats. To ensure our segmentation analysis was reliable and repeatable, interscan and interanimal variability were assessed with intraclass correlation coefficients (ICC) and 95% confidence intervals by using IBM (Armonk, NY, USA) SPSS Statistics Version 24 (Tables 1, 2).[41,42] To calculate interscan variability, three repeated scan measurements from three different P30 RCS rats were correlated (Table 1). To calculate the variation of OD and OS scans, measurements from nine different P30 RCS rats were correlated (Table 2).

Total retina, INL, ONL+, RPE, and HRL thicknesses (micrometers, *y*-axis) were measured −40° outward in the inferior (OD and OS), nasal (OS), or temporal (OD) direction and +40° outward in the superior (OD and OS), nasal (OD), or temporal (OS) direction from the optic nerve head (*x*-axis). The resulting waves for TR and ONL+ in the superior and inferior retina were averaged and plotted as spider graphs. Additionally, points from −40° to −25° and 25° to 40° were averaged to obtain TR, INL, ONL+, RPE, and HRL thicknesses for each eye in each quadrant. Right and left eye thicknesses were averaged and plotted against age (days) for all of the animals scanned. Best-fit equations were generated by using GraphPad (GraphPad Software, Inc., La Jolla, CA, USA) Prism 7 software and plotted for each data set. A 2-way ANOVA, multiple comparisons test was used to compare average RCS retinal layer thickness between each quadrant at each time point. A P value of ≤ 0.01 was considered significant.

Histology

Before enucleation, the superior edge of the eye was marked. Once enucleated, eyes were placed immediately in PREFER, a glyoxal fixative (Anatech Ltd, Battle Creek, MI, USA) and incubated overnight at room temperature. Eyes were then placed in cassettes and stored in 70% ethanol at room temperature. Orientated eyes were processed and embedded in paraffin for sectioning (Tissue-Tek VIP 6, Tissue-Tek TEC 5; Sakura Finetek USA, Inc., Torrance, CA, USA). Sections were cut with a microtome to a thickness of 4 μm, stained with hematoxylin-eosin (H&E), and viewed on a Leica DMI3000 B microscope (Leica Microsystems GmbH, Wetzlar, Germany). All images were taken at a magnification of ×40.

Results

Qualitative SD-OCT Analysis

Retinal layers including the ganglion cell layer (GCL), inner plexiform layer (IPL), INL, OPL, ONL, OLM, photoreceptor inner and outer segments (PR), and RPE were clearly visible in SD-OCT images of LE rats at all ages examined (Fig. 1). In the RCS retina, the ellipsoid zone (EZ), which consists of

Investigative Ophthalmology & Visual Science

Table 1. Reproducibility of First, Second, and Third Scan Retinal Layer Thickness Measurements

	RCS P30 OD		RCS P30 OS	
Retinal Layer and Location	**Intraclass Correlation Coefficient**	**95% Confidence Interval**	**Intraclass Correlation Coefficient**	**95% Confidence Interval**
Total retina				
Superior	0.996	0.971 to 1.000	0.842	−0.925 to 0.996
Inferior	0.988	0.913 to 1.000	0.989	0.872 to 1.000
Nasal	0.997	0.980 to 1.000	0.898	0.327 to 0.997
Temporal	1.000	0.997 to 1.000	0.941	0.507 to 0.998
Inner nuclear layer				
Superior	0.385	4.755 to 0.988	−0.012	−0.825 to 0.949
Inferior	0.813	−0.315 to 0.995	0.564	−0.541 to 0.987
Nasal	−0.504	9.090 to 0.970	0.559	−1.607 to 0.988
Temporal	0.963	0.721 to 0.999	0.641	17.079 to 0.992
Outer nuclear layer+				
Superior	0.977	0.835 to 0.999	0.931	0.389 to 0.998
Inferior	0.648	−0.440 to 0.990	0.889	0.279 to 0.997
Nasal	0.778	−0.334 to 0.994	0.742	35.011 to 0.994
Temporal	0.944	0.197 to 0.999	0.929	0.492 to 0.998
Retinal pigment epithelium				
Superior	0.526	−3.318 to 0.988	−0.118	−2.017 to 0.959
Inferior	0.398	−0.984 to 0.981	0.816	−1.482 to 0.996
Nasal	0.953	0.664 to 0.999	0.657	−0.538 to 0.990
Temporal	0.435	−2.219 to 0.985	0.743	−0.698 to 0.983
Hyperreflective layer				
Superior	0.937	0.542 to 0.998	0.852	0.134 to 0.996
Inferior	0.985	0.887 to 1.000	0.905	0.287 to 0.998
Nasal	0.564	−0.941 to 0.988	0.447	−0.813 to 0.983
Temporal	0.841	0.103 to 0.996	0.519	−1.077 to 0.986

mitochondria within the ellipsoid layer of the outer portion of the inner segments and represents the inner/outer segment junction, could be identified from P17 to P23, but the outer segments (OS) were becoming hyperreflective, which caused them to become isoreflective with the EZ. Thus, differentiation between the EZ and OS was less distinct in P17 to P23 RCS retinas than in LE controls. By P30, the PR and OLM were indistinguishable and isoreflective. Thus, from P30 to P90, this area of the retina was observed as a single layer and termed "the hyperreflective layer" (HRL). From P30 to P60 the ONL became progressively hyperreflective and thinned relative to baseline. By P45, it became isoreflective with the OPL and became difficult to distinguish, but was not detectable by P90 (Fig. 1).

Quantitative SD-OCT Analysis

To characterize the progressive retinal degeneration in the RCS rat, manual segmentation was performed to calculate TR, INL, ONL+, HRL, RPE thickness (see schematic for segmentation lines in figure legend; Fig. 2A). To validate our segmentation analysis, interscan and interanimal variability were assessed with ICC (Tables 1, 2).[41,42] Our manual segmentation provided reproducible retinal layer thickness measurements, as most thickness measurements, obtained from three individual scans, were correlative (ICC = 0.5–1; Table 1). There was also good correlation (ICC = 0.644–0.944) between retinal layer thickness measurements obtain from right and left eyes of P30 RCS rats, suggesting that degeneration rates were consistent between eyes (Table 2).

Retinal layers and segmentation remained consistent from P30 to P90 in LE rats. In RCS rats, segmentation changed at P30 due to the appearance of the HRL and at P90 due to the loss of the ONL+ (Fig. 2A). Scatter plots of average TR and ONL+ thickness obtained from RCS rats over time demonstrated considerable declines that were best fit, based on R^2 values, with exponential decay functions (Fig. 2B; Supplementary Table S1). In contrast, all other retinal layers quantified in both RCS rats and LE controls were best fit with linear functions (Fig. 2B; Supplementary Table S1). These data demonstrated that total retinal degeneration in the RCS rat was primarily due to the loss of photoreceptors, which is highlighted in Figure 3. Spider graphs of the superior and inferior retina illustrate that average TR and ONL+ thickness decreased consistently over time in the RCS rat, whereas LE rats had a narrow range in average TR and ONL+ thickness from P30 to P90 (Fig. 3, gray shading). Scatter plots in Figure 2 also demonstrated the consistency of retinal layer thickness between the different retinal quadrants. The most noticeable deviation was the HRL thickness in the RCS rat. Superior HRL thickness was significantly increased as compared to nasal, temporal, and inferior HRL thickness from P30 to P56 (Fig. 2B, Supplementary Table S2; $P \leq 0.01$). At P60, superior HRL thickness was still significantly increased as compared to temporal and inferior HRL thickness. By P90, HRL thickness was not significantly different in any retinal quadrant (Fig. 2B, Supplementary Table S2; $P \leq 0.01$). Not surprisingly, average superior TR thickness was affected and was also significantly increased as compared to nasal, temporal, and inferior TR thickness from P30 to P37 (Fig. 2B, Supplementary Table S2; $P \leq 0.01$). Interestingly, superior ONL+ was thicker than all other retinal quadrants at P37 (Fig. 2B, Supplementary Table S2; $P \leq 0.01$).

Investigative Ophthalmology & Visual Science

Table 2. Retinal Layer Thickness Variation Between RCS OD and OS Scans at P30

Retinal Layer and Location	Intraclass Correlation Coefficient, $n = 9$	95 % Confidence Interval, $n = 9$
Total retina		
Superior	0.724	−0.104 to 0.936
Inferior	0.797	0.123 to 0.954
Nasal	0.869	0.437 to 0.970
Temporal	0.711	−0.89 to 0.932
Inner nuclear layer		
Superior	0.756	−0.004 to 0.944
Inferior	−1.495	−10.822 to 0.461
Nasal	0.796	0.019 to 0.955
Temporal	0.679	−0.627 to 0.930
Outer nuclear layer+		
Superior	0.743	−0.091 to 0.942
Inferior	0.699	−0.250 to 0.931
Nasal	0.466	−1.764 to 0.883
Temporal	0.756	−0.002 to 0.945
Retinal pigment epithelium		
Superior	0.814	0.142 to 0.958
Inferior	0.944	0.751 to 0.987
Nasal	0.644	−0.485 to 0.919
Temporal	0.830	0.200 to 0.962
Hyperreflective layer		
Superior	0.741	0.023 to 0.939
Inferior	0.203	−3.830 to 0.831
Nasal	0.325	−3.036 to 0.856
Temporal	0.668	−0.713 to 0.927

Histology and SD-OCT Image Comparison

Histology of retinal sections from P21, P30, P45, and P60 RCS rats was compared to locally matched SD-OCT images (Fig. 4). At P21 the GCL, INL, OPL, ONL, PR, and RPE were clearly observable in both histology and SD-OCT images. At this age, OS disorganization was only evident at the apical side of the RPE. By P30, OS disorganization expanded and the correlation between the PR/debris layer and the HRL was evident, suggesting that both layers are comprised of IS, disorganized OS, and debris (Fig. 4B). Furthermore, both modalities demonstrated that this layer is thicker in the superior retina and thins over time (Fig. 4). By P45 the ONL has significantly degenerated and less than half of the ONL remained, which was clearly visible in the histology images. In the SD-OCT images, the ONL became hyperreflective, isoreflective with the OPL, and was more difficult to distinguish than in the retinal sections (Fig. 4C). By P60, the ONL contained approximately three rows of cell nuclei. Although the ONL resolution declined with disease progression, an ONL+ layer was still measurable in SD-OCT images at this time point (Fig. 4D). When comparing the histology and SD-OCT images from P21 to P60, both demonstrated an observable decrease in TR and ONL thickness (Fig. 4).

Discussion

This study provides the first in vivo quantification of RCS retinal degeneration longitudinally. Spectral-domain OCT allowed for high-resolution imaging of RCS retinal structure and quantification of retinal layers including TR, INL, ONL+, RPE, and HRL. Total retina and ONL+ thickness degenerated over time, and the loss of the ONL+ accounted primarily for TR reduction (Fig. 3). Thus, the comprehensive TR and ONL+ thickness measurements can be used as a baseline for future studies that assess the efficacy of potential therapies for outer retinal degeneration in the RCS rat. In addition, HRL thickness, which correlated to IS, disorganized OS, and debris accumulation observed in histology (Fig. 4), can also be used to assess photoreceptor changes longitudinally.

When comparing our SD-OCT analysis to previous published anatomic measurements, we found that thickness values differed, but the rate of thickness changes was consistent.[8] For example, both SD-OCT and anatomic assessments show that half the ONL thickness is decreased by approximately 7 weeks of age, that ONL thinning occurs at a uniform rate in all four quadrants, and that the ONL becomes absent in many areas of the posterior retina.[8] However, manual segmentation of the ONL+ resulted in thicker measurements than in previous reports, which measured distinctly around photoreceptor cell bodies (e.g., SD-OCT at P17: ONL+ ∼90 μm, tissue at P17: ONL ∼50 μm).[8] This difference seems reasonable for two main reasons: (1) histologic processing is known to dehydrate the tissue; and (2) our reported ONL+ measurement included OPL thickness, whereas ONL measurements from previous anatomic reports do not include OPL thickness.[8]

Hyperreflective layer thickness, acquired from SD-OCT images, and an outer segment layer (OSL) thickness, acquired from previous anatomic assessments, were also comparable.[8] The OSL has been quantified in order to estimate the relative volume of OS debris accumulation during photoreceptor degeneration.[8,9] In a previous anatomic assessment, it is reported that the OSL thickness increases with age, but after maximum thickness is reached at P35, the OSL decreases with progressive degeneration.[8] In addition, the OSL thickness is consistently thicker in the superior retina.[8] These results seem comparable to the HRL identified in the RCS retina with SD-OCT. The HRL was fully formed and at its peak thickness at P30. Hyperreflective layer thickness then decreased with progressive degeneration and was consistently thicker in the superior retina. Quantification of the HRL in SD-OCT images resulted in thicker values than in the quantification of the OSL in retinal sections (e.g., SD-OCT at P37 superior: HRL ∼61 μm, tissue at P35 superior: OSL/debris layer ∼48 μm).[8] Two main reasons could account for this discrepancy: (1) the OSL measured on retinal sections may not include the inner segment thickness; and (2) as the hyperreflectivity increased and the OLM became less distinct, it is possible that the HRL may include cells from the ONL. Overall, the HRL correlated with the PR/debris layer in our histology images (Fig. 4), thus we suggest the HRL can be used to quantify photoreceptor inner and outer segment changes longitudinally.

Many histologic changes could be responsible for generating the HRL, including disorganization of OS discs resulting in lamellar whorls of membranes, the expansion or swelling of apical RPE processes, or invasion of macrophages into the outer retina.[9] What remains unclear is the causation of increased thickness in the superior retina. Previous reports[8] suggest that increased debris forms from an increase in photoreceptor cell bodies. Our data demonstrated a correlation between preservation of ONL+ thickness and increased HRL thickness in the superior retina from P30 to P37 (Supplementary Table S2), which supports this hypothesis.

Histologic analysis of retinal tissue has been considered the gold standard for characterizing retinal degeneration and assessing the efficacy of potential treatments for AMD and inherited retinal dystrophies in the RCS rat.[8,12,26,43–46] However, histologic processing precludes the ability to perform longitudinal analysis, thus increasing the number of animals

Investigative Ophthalmology & Visual Science

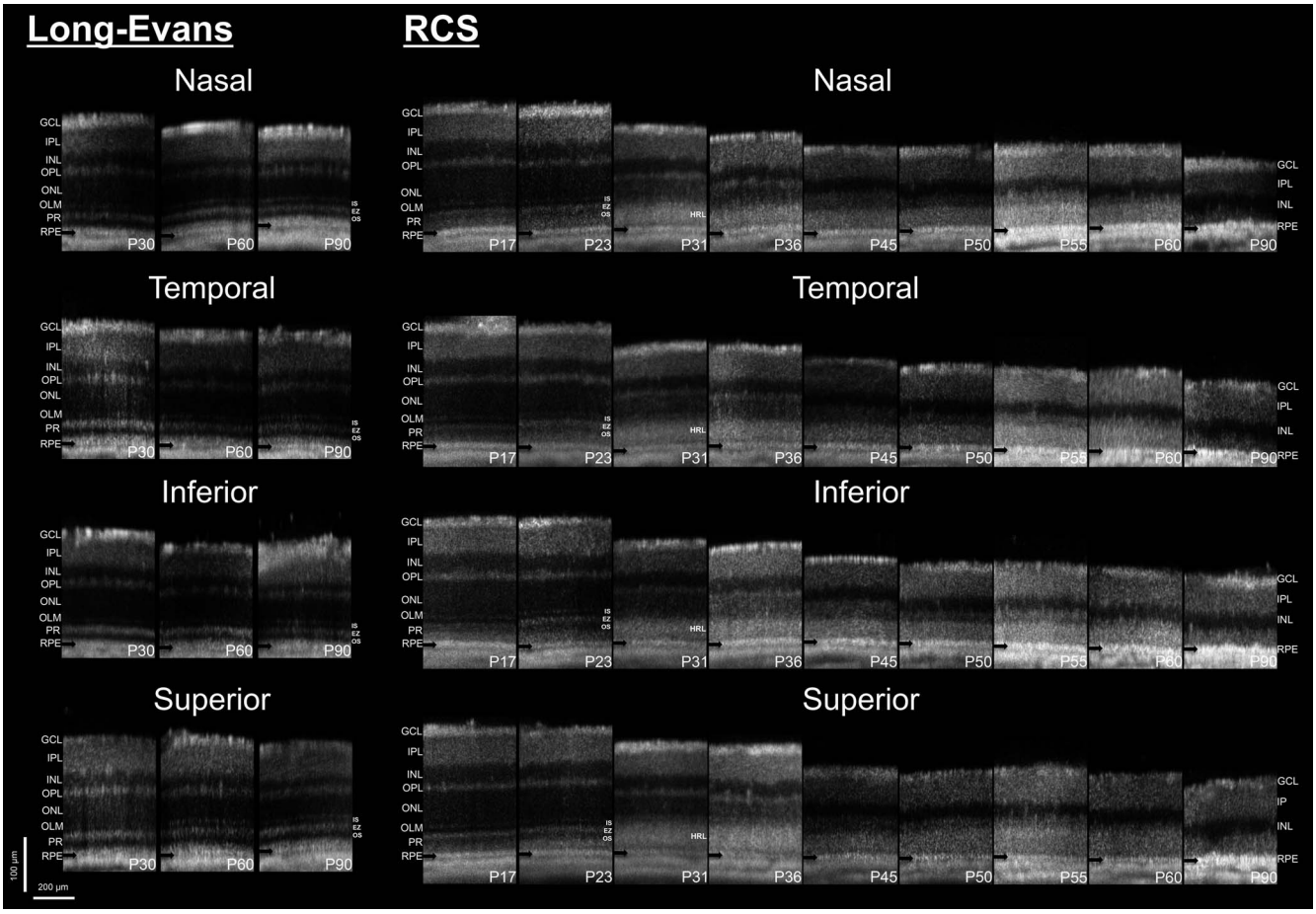

Figure 1. Images acquired with SD-OCT illustrate the longitudinal retinal degeneration in the RCS rat. Representative linear SD-OCT scans from right eyes of Long-Evans and RCS rats at differing ages from P17 to P90. Images are representative of the same location in both Long-Evans and RCS retinas, approximately 30° from the optic nerve head in each retinal quadrant. Each image is approximately 2°. Photoreceptors were maintained in Long-Evans retinas and degenerated over time in RCS retinas. *Black arrow* defines RPE layer. IS, inner segments; ONL, outer nuclear layer; OS, outer segments.

required for long-term studies. In addition, artifacts from postmortem processing are unavoidable, including fixation and dehydration, which can alter layer thicknesses and mask features of in vivo disease progression. Noninvasive, high-resolution SD-OCT imaging offers an alternative in vivo approach to obtaining structural measurements of disease progression.[30] Spectral-domain OCT imaging has been validated in multiple mouse (*Rho*$^{-/-}$, *Rpe65*$^{-/-}$, *rd1*, *rd10*) and rat (Rho P23H) inherited retinal degeneration models.[32–34] These studies have consistently reported that SD-OCT is able to capture morphologic changes during disease progression and that SD-OCT thickness measurements are notably higher, but in strong correlation with anatomic thickness measurements.[32–34] In addition, SD-OCT has been able to image well-characterized phenotypes, as in the complete absence of rod OS in the *Rho*$^{-/-}$ mouse,[34] and reveal novel in vivo findings that lead to discoveries about disease progression. For example, *Rpe65*$^{-/-}$ mice have less distinct laminar organization, leading to the conclusion that expression of cytoskeletal elements and components of the extracellular matrix may be modified and playing a role in disease progression.[34] In a study that characterized and revealed differences in disease progression between the *rd1* and *rd10* mice, retinal separations, often thought to be an artifact of histologic processing, were observed in the *rd10* mice by SD-OCT, confirming their in vivo existence.[32] Because of these findings, multiple studies now use retinal thickness measurements obtained from SD-OCT images to demonstrate the long-term efficacy of various adeno-associated virus gene therapies for various inherited retinal degeneration mouse models (*rd1*, *rd10*, P23H Rho$^{+/-}$, *Rs1h*$^{-/-}$, *rd12*).[35–38] Despite the existing validation of SD-OCT and numerous software programs available for segmentation of the retina,[47–52] ONL counts from H&E-stained retinal sections continue to be the main methodology used to illustrate preservation of photoreceptors after therapeutic interventions in the RCS rat.[43–46] The congruency between histologic analysis and SD-OCT analysis demonstrated in this study suggests that SD-OCT may also be used to quantify the efficacy of various therapies longitudinally.

We demonstrated that SD-OCT overcomes the challenge of longitudinal anatomic assessments; however, some limitations of this technology remain. The SD-OCT analysis performed in this study was restricted to the posterior retina (up to 40° from the optic nerve head).[32] As photoreceptor degeneration rates differ between posterior and peripheral retina in the RCS rat,[8] this study should be used primarily as a reference for interpreting data from the posterior retina, while recognizing that rates of degeneration can differ in the peripheral retina. Although SD-OCT offers high-resolution imaging, manual segmentation of the ONL became challenging during the course of degeneration. The ONL became hyperreflective over time, slowly becoming isoreflective with the OPL, OLM, and

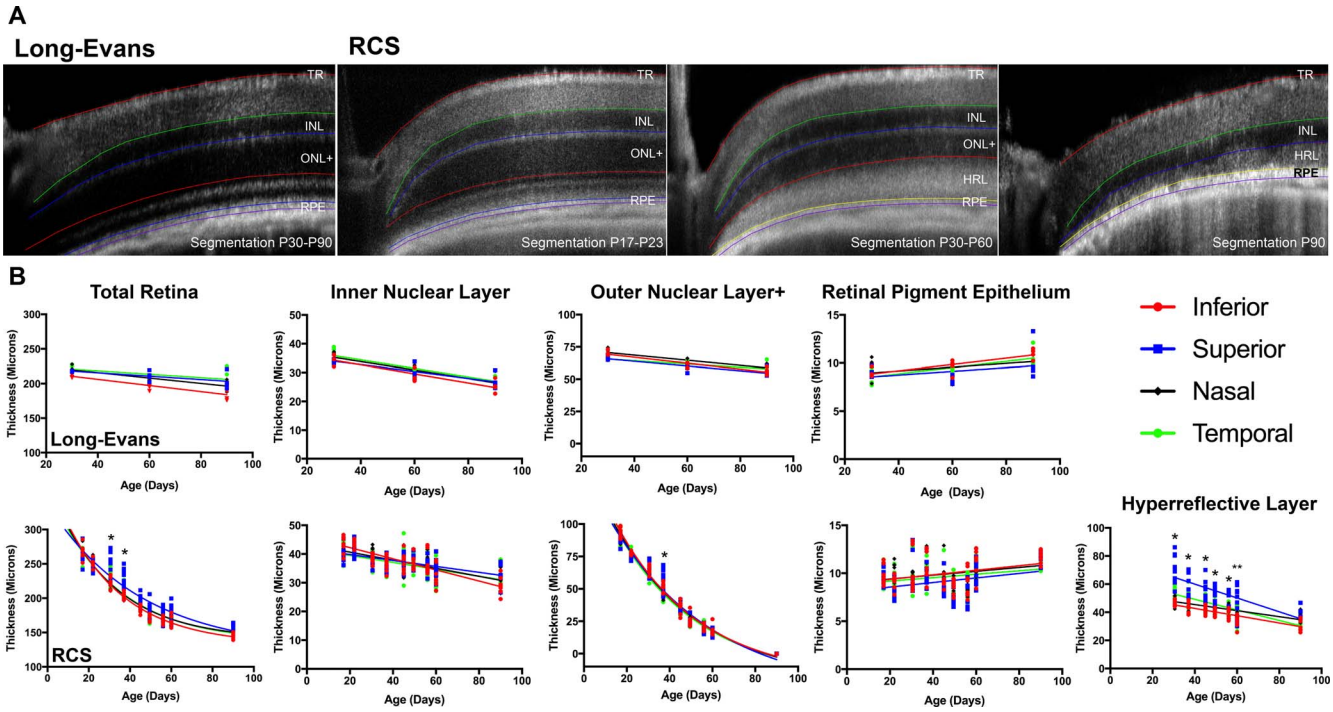

Figure 2. Segmentation allows for longitudinal quantification of retinal degeneration in the RCS rat. (**A**) Representative linear SD-OCT scans of superior retina from right eyes of Long-Evans and RCS rats. Retinal layers were distinguished by manual segmentation using IGOR Pro software. Schematic for segmentation lines: TR, *bottom purple line* to the *top red line*; INL, *blue line* to the *green line* that surround the INL label; outer nuclear layer plus outer plexiform layer (ONL+), *red line* to *blue line* that surround the ONL+ label; RPE, *purple line* to the *blue line* (LE P30–P90 and RCS P17–P23) or *purple line* to the *yellow line* (RCS P30–P90) that surround RPE label; HRL, *yellow line* to the *red line* (RCS P30–P60) or *yellow line* to the *blue line* (RCS P90) that surround HRL label. (**B**) Right eye and left eye TR, ONL+, INL, RPE, and HRL thicknesses from Long-Evans and RCS retinas in each retinal quadrant were averaged and plotted against age. RCS TR and ONL+ degeneration was best fit with an exponential decay function, whereas all other data points were best fit with linear regressions. A 2-way ANOVA, multiple comparisons test was used to compare average RCS retinal layer thickness between each quadrant at each time point. *Thickness of the superior retina was significantly increased compared to all other quadrants at specified age ($P \leq 0.01$). **Thickness of the superior retina was significantly increased compared to temporal and inferior retina at specified age ($P \leq 0.01$). Long-Evans: $N = 4$ animals; RCS: $N = 7$–10 animals.

HRL, which made it difficult to distinguish. To address this limitation, we used an ONL+ measurement, which contained both the ONL and OPL. However, since the OLM became difficult to discern, this did not account for any ONL that may have been masked by the HRL.

Although the RPE was observable in SD-OCT images, the segmentation analysis showed appreciable variation between the animals. The outline of the RPE was clear in some images and less distinguished in others owing to hyperreflectance of the sclera and HRL. It is well known that the RPE is maintained in the RCS rat,[8] but we hypothesized that due to RPE dysfunction there may be measurable changes in its thickness. Our analysis suggests that if RPE thickness is changing during photoreceptor degeneration, better resolution imaging would be required to get consistent measurements of such a thin monolayer of cells.

The RCS rat has been and will continue to be a fundamental model used to develop therapies for AMD and inherited retinal dystrophies.[21,23,25,43–46,53–56] We used SD-OCT to quantify thickness of retinal layers in the RCS rat throughout the course of degeneration. Spectral-domain OCT is an important complement to histology and in many cases could be used as a

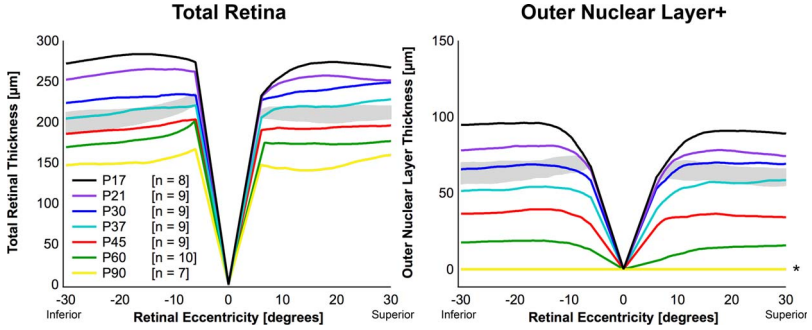

Figure 3. RCS photoreceptor degeneration is primarily responsible for reduction in total retinal thickness. RCS total retina and ONL+ thicknesses obtained from right eye and left eye inferior and superior SD-OCT scans were averaged and plotted versus retinal eccentricity from the optic nerve head. Outer nuclear layer+ degeneration corresponds with observed total retina loss over time. *Gray shading* represents Long-Evans total retina and ONL+ range from P30 to P90. RCS ONL+ is undetectable by SD-OCT at P90 and thus is plotted as zero (*).

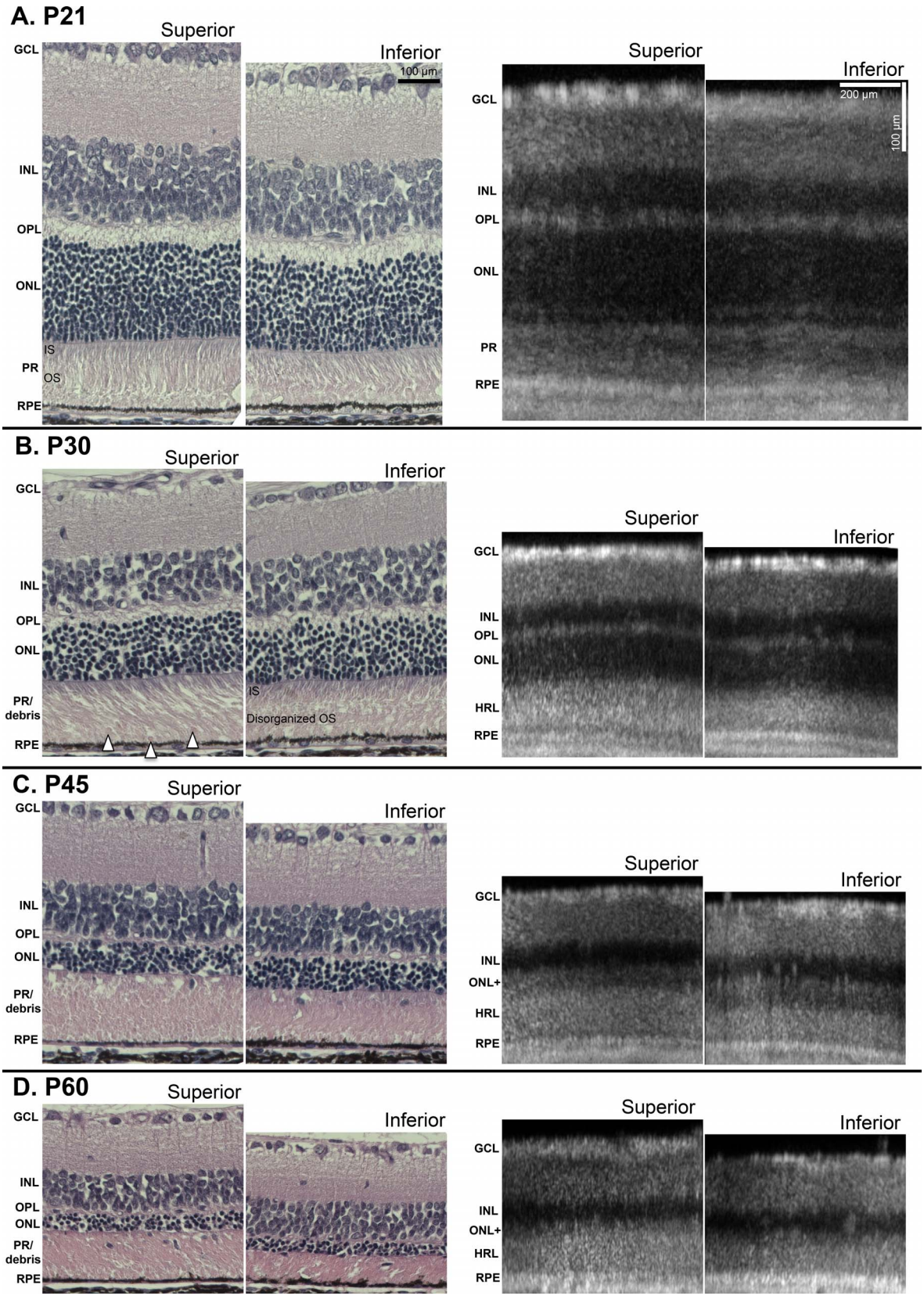

Figure 4. Histology and SD-OCT comparison. Representative histology and SD-OCT images of superior and inferior quadrants of the posterior retina from right eyes of RCS rats at P21 (**A**), P30 (**B**), P45 (**C**), and P60 (**D**). Histology and SD-OCT images demonstrate RCS photoreceptor degeneration over time. The HRL correlates with the PR/debris layer indicating a composition of IS, disorganized OS, and debris (*arrowheads*).

Investigative Ophthalmology & Visual Science

surrogate when assessing the efficacy of treatments for outer retinal degeneration in the RCS rat.

Acknowledgments

The authors thank Michael Gale for assistance with manual segmentation.

Supported by unrestricted departmental funding from Research to Prevent Blindness (New York, NY, USA), Grant P30 EY010572 from the National Institutes of Health (Bethesda, MD, USA), K08 Career Development Award (K08 EY021186, MEP), Alcon Young Investigator Award (MEP), Foundation Fighting Blindness Enhanced Research and Clinical Training Award (CD-NMT-0914-0659-OHSU, MEP), Career Development Award from Research to Prevent Blindness (MEP), Sybil B. Harrington Special Scholar Award from Research to Prevent Blindness (TJM), Oregon Clinical and Translational Research Institute (OCTRI).

Disclosure: **R.C. Ryals**, None; **M.D. Andrews**, None; **S. Datta**, None; **A.S. Coyner**, None; **C.M. Fischer**, None; **Y. Wen**, None; **M.E. Pennesi**, None; **T.J. McGill**, None

References

1. Gheorghe A, Mahdi L, Musat O. Age-related macular degeneration. *Rom J Ophthalmol*. 2015;59:74–77.
2. Sahel JA, Marazova K, Audo I. Clinical characteristics and current therapies for inherited retinal degenerations. *Cold Spring Harb Perspect Med*. 2015;5:a017111.
3. Daiger SP, Bowne SJ, Sullivan LS. Perspective on genes and mutations causing retinitis pigmentosa. *Arch Ophthalmol*. 2007;125:151–158.
4. Pang JJ, Chang B, Kumar A, et al. Gene therapy restores vision-dependent behavior as well as retinal structure and function in a mouse model of RPE65 Leber congenital amaurosis. *Mol Ther*. 2006;13:565–572.
5. Acland GM, Aguirre GD, Ray J, et al. Gene therapy restores vision in a canine model of childhood blindness. *Nat Genet*. 2001;28:92–95.
6. Gal A, Li Y, Thompson DA, et al. Mutations in MERTK, the human orthologue of the RCS rat retinal dystrophy gene, cause retinitis pigmentosa. *Nat Genet*. 2000;26:270–271.
7. LaVail MM, Mullen RJ. Role of the pigment epithelium in inherited retinal degeneration analyzed with experimental mouse chimeras. *Exp Eye Res*. 1976;23:227–245.
8. LaVail MM, Battelle BA. Influence of eye pigmentation and light deprivation on inherited retinal dystrophy in the rat. *Exp Eye Res*. 1975;21:167–192.
9. Matthes MT, LaVail MM. Inherited retinal dystrophy in the RCS rat: composition of the outer segment debris zone. *Prog Clin Biol Res*. 1989;314:315–330.
10. McGill TJ, Douglas RM, Lund RD, Prusky GT. Quantification of spatial vision in the Royal College of Surgeons rat. *Invest Ophthalmol Vis Sci*. 2004;45:932–936.
11. McGill TJ, Lund RD, Douglas RM, et al. Syngeneic Schwann cell transplantation preserves vision in RCS rat without immunosuppression. *Invest Ophthalmol Vis Sci*. 2007;48:1906–1912.
12. Mullen RJ, LaVail MM. Inherited retinal dystrophy: primary defect in pigment epithelium determined with experimental rat chimeras. *Science*. 1976;192:799–801.
13. Wang S, Lu B, Lund RD. Morphological changes in the Royal College of Surgeons rat retina during photoreceptor degeneration and after cell-based therapy. *J Comp Neurol*. 2005;491:400–417.
14. Zambarakji HJ, Keegan DJ, Holmes TM, et al. High resolution imaging of fluorescein patterns in RCS rat retinae and their direct correlation with histology. *Exp Eye Res*. 2006;82:164–171.
15. LaVail MM. Photoreceptor characteristics in congenic strains of RCS rats. *Invest Ophthalmol Vis Sci*. 1981;20:671–675.
16. Villegas-Perez MP, Lawrence JM, Vidal-Sanz M, Lavail MM, Lund RD. Ganglion cell loss in RCS rat retina: a result of compression of axons by contracting intraretinal vessels linked to the pigment epithelium. *J Comp Neurol*. 1998;392:58–77.
17. Eisenfeld AJ, LaVail MM, LaVail JH. Assessment of possible transneuronal changes in the retina of rats with inherited retinal dystrophy: cell size, number, synapses, and axonal transport by retinal ganglion cells. *J Comp Neurol*. 1984;223:22–34.
18. Pavlidis M, Fischer D, Thanos S. Photoreceptor degeneration in the RCS rat attenuates dendritic transport and axonal regeneration of ganglion cells. *Invest Ophthalmol Vis Sci*. 2000;41:2318–2328.
19. Deng WT, Dinculescu A, Li Q, et al. Tyrosine-mutant AAV8 delivery of human MERTK provides long-term retinal preservation in RCS rats. *Invest Ophthalmol Vis Sci*. 2012;53:1895–1904.
20. Vollrath D, Feng W, Duncan JL, et al. Correction of the retinal dystrophy phenotype of the RCS rat by viral gene transfer of Mertk. *Proc Natl Acad Sci U S A*. 2001;98:12584–12589.
21. LaVail MM. Legacy of the RCS rat: impact of a seminal study on retinal cell biology and retinal degenerative diseases. *Prog Brain Res*. 2001;131:617–627.
22. LaVail MM, Yasumura D, Matthes MT, et al. Gene therapy for MERTK-associated retinal degenerations. *Adv Exp Med Biol*. 2016;854:487–493.
23. McGill TJ, Cottam B, Lu B, et al. Transplantation of human central nervous system stem cells - neuroprotection in retinal degeneration. *Eur J Neurosci*. 2012;35:468–477.
24. Carr AJ, Vugler AA, Hikita ST, et al. Protective effects of human iPS-derived retinal pigment epithelium cell transplantation in the retinal dystrophic rat. *PLoS One*. 2009;4:e8152.
25. Lavail MM, Li L, Turner JE, Yasumura D. Retinal pigment epithelial cell transplantation in RCS rats: normal metabolism in rescued photoreceptors. *Exp Eye Res*. 1992;55:555–562.
26. Li LX, Turner JE. Inherited retinal dystrophy in the RCS rat: prevention of photoreceptor degeneration by pigment epithelial cell transplantation. *Exp Eye Res*. 1988;47:911–917.
27. Sauve Y, Klassen H, Whiteley SJ, Lund RD. Visual field loss in RCS rats and the effect of RPE cell transplantation. *Exp Neurol*. 1998;152:243–250.
28. McGill TJ, Prusky GT, Douglas RM, et al. Discordant anatomical, electrophysiological, and visual behavioral profiles of retinal degeneration in rat models of retinal degenerative disease. *Invest Ophthalmol Vis Sci*. 2012;53:6232–6244.
29. Huang D, Swanson EA, Lin CP, et al. Optical coherence tomography. *Science*. 1991;254:1178–1181.
30. Swanson EA, Izatt JA, Hee MR, et al. In vivo retinal imaging by optical coherence tomography. *Opt Lett*. 1993;18:1864–1866.
31. Hee MR, Izatt JA, Swanson EA, et al. Optical coherence tomography of the human retina. *Arch Ophthalmol*. 1995;113:325–332.
32. Pennesi ME, Michaels KV, Magee SS, et al. Long-term characterization of retinal degeneration in rd1 and rd10 mice using spectral domain optical coherence tomography. *Invest Ophthalmol Vis Sci*. 2012;53:4644–4656.
33. Cuenca N, Fernandez-Sanchez L, Sauve Y, et al. Correlation between SD-OCT, immunocytochemistry and functional findings in an animal model of retinal degeneration. *Front Neuroanat*. 2014;8:151.

Investigative Ophthalmology & Visual Science

34. Huber G, Beck SC, Grimm C, et al. Spectral domain optical coherence tomography in mouse models of retinal degeneration. *Invest Ophthalmol Vis Sci*. 2009;50:5888–5895.
35. Mao H, Gorbatyuk MS, Rossmiller B, Hauswirth WW, Lewin AS. Long-term rescue of retinal structure and function by rhodopsin RNA replacement with a single adeno-associated viral vector in P23H RHO transgenic mice. *Hum Gene Ther*. 2012;23:356–366.
36. Pang JJ, Dai X, Boye SE, et al. Long-term retinal function and structure rescue using capsid mutant AAV8 vector in the rd10 mouse, a model of recessive retinitis pigmentosa. *Mol Ther*. 2011;19:234–242.
37. Dalkara D, Byrne LC, Klimczak RR, et al. In vivo-directed evolution of a new adeno-associated virus for therapeutic outer retinal gene delivery from the vitreous. *Sci Transl Med*. 2013;5:189ra176.
38. Dai X, Han J, Qi Y, et al. AAV-mediated lysophosphatidylcholine acyltransferase 1 (Lpcat1) gene replacement therapy rescues retinal degeneration in rd11 mice. *Invest Ophthalmol Vis Sci*. 2014;55:1724–1734.
39. Feng L, Sun Z, Han H, Zhou Y, Zhang M. No age-related cell loss in three retinal nuclear layers of the Long-Evans rat. *Vis Neurosci*. 2007;24:799–803.
40. LaVail MM, Lawson NR. Development of a congenic strain of pigmented and albino rats for light damage studies. *Exp Eye Res*. 1986;43:867–869.
41. Lee S, Fallah N, Forooghian F, et al. Comparative analysis of repeatability of manual and automated choroidal thickness measurements in nonneovascular age-related macular degeneration. *Invest Ophthalmol Vis Sci*. 2013;54:2864–2871.
42. Ho J, Sull AC, Vuong LN, et al. Assessment of artifacts and reproducibility across spectral- and time-domain optical coherence tomography devices. *Ophthalmology*. 2009;116:1960–1970.
43. Cuenca N, Fernandez-Sanchez L, McGill TJ, et al. Phagocytosis of photoreceptor outer segments by transplanted human neural stem cells as a neuroprotective mechanism in retinal degeneration. *Invest Ophthalmol Vis Sci*. 2013;54:6745–6756.
44. Lu B, Malcuit C, Wang S, et al. Long-term safety and function of RPE from human embryonic stem cells in preclinical models of macular degeneration. *Stem Cells*. 2009;27:2126–2135.
45. Riera M, Fontrodona L, Albert S, et al. Comparative study of human embryonic stem cells (hESC) and human induced pluripotent stem cells (hiPSC) as a treatment for retinal dystrophies. *Mol Ther Methods Clin Dev*. 2016;3:16010.
46. Thomas BB, Zhu D, Zhang L, et al. Survival and functionality of hESC-derived retinal pigment epithelium cells cultured as a monolayer on polymer substrates transplanted in RCS rats. *Invest Ophthalmol Vis Sci*. 2016;57:2877–2887.
47. Markand S, Saul A, Roon P, et al. Retinal ganglion cell loss and mild vasculopathy in methylene tetrahydrofolate reductase (Mthfr)-deficient mice: a model of mild hyperhomocysteinemia. *Invest Ophthalmol Vis Sci*. 2015;56:2684–2695.
48. Brandao LM, Ledolter AA, Schotzau A, Palmowski-Wolfe AM. Comparison of two different OCT systems: retina layer segmentation and impact on structure-function analysis in glaucoma. *J Ophthalmol*. 2016;2016:8307639.
49. Sonka M, Abramoff MD. Quantitative analysis of retinal OCT. *Med Image Anal*. 2016;33:165–169.
50. Tian J, Varga B, Somfai GM, Lee WH, Smiddy WE, DeBuc DC. Real-time automatic segmentation of optical coherence tomography volume data of the macular region. *PLoS One*. 2015;10:e0133908.
51. Seigo MA, Sotirchos ES, Newsome S, et al. In vivo assessment of retinal neuronal layers in multiple sclerosis with manual and automated optical coherence tomography segmentation techniques. *J Neurol*. 2012;259:2119–2130.
52. Knott EJ, Sheets KG, Zhou Y, Gordon WC, Bazan NG. Spatial correlation of mouse photoreceptor-RPE thickness between SD-OCT and histology. *Exp Eye Res*. 2011;92:155–160.
53. Conlon TJ, Deng WT, Erger K, et al. Preclinical potency and safety studies of an AAV2-mediated gene therapy vector for the treatment of MERTK associated retinitis pigmentosa. *Hum Gene Ther Clin Dev*. 2013;24:23–28.
54. Ghazi NG, Abboud EB, Nowilaty SR, et al. Treatment of retinitis pigmentosa due to MERTK mutations by ocular subretinal injection of adeno-associated virus gene vector: results of a phase I trial. *Hum Genet*. 2016;135:327–343.
55. Hu Y, Liu L, Lu B, et al. A novel approach for subretinal implantation of ultrathin substrates containing stem cell-derived retinal pigment epithelium monolayer. *Ophthalmic Res*. 2012;48:186–191.
56. Ilmarinen T, Hiidenmaa H, Koobi P, et al. Ultrathin polyimide membrane as cell carrier for subretinal transplantation of human embryonic stem cell derived retinal pigment epithelium. *PLoS One*. 2015;10:e0143669.

Investigative Ophthalmology & Visual Science